JGR Space Physics

RESEARCH ARTICLE
10.1029/2020JA028198

New Insights From Long-Term Measurements of Inner Belt Protons (10s of MeV) by SAMPEX, POES, Van Allen Probes, and Simulation Results

Xinlin Li[1,2], Zheng Xiang[3,1], Kun Zhang[1,2], Lengying Khoo[1,2], Hong Zhao[1], Daniel N. Baker[1], and Michael A. Temerin[4]

[1]Laboratory for Atmospheric and Space Physics, University of Colorado Boulder, Boulder, CO, USA, [2]Department of Aerospace Engineering Sciences, University of Colorado Boulder, Boulder, CO, USA, [3]Department of Space Physics, School of Electronic Information, Wuhan University, Wuhan, China, [4]Space Sciences Lab, University of California Berkeley, Berkeley, CA, USA

Key Points:
- The solar cycle variation of inner belt protons measured by LEO satellites is mainly due to losses from atmospheric collisions
- Inner belt proton intensity and variation measured at LEO sensitively depend on the altitude above the SAA
- Measurements and simulations reveal a strong spatial gradient of trapped protons mirroring near the magnetic equator below $L = 1.2$

Correspondence to:
X. Li,
lix@lasp.colorado.edu

Citation:
Li, X., Xiang, Z., Zhang, K., Khoo, L., Zhao, H., Baker, D. N., & Temerin, M. A. (2020). New insights from long-term measurements of inner belt protons (10s of MeV) by SAMPEX, POES, Van Allen Probes, and simulation results. *Journal of Geophysical Research: Space Physics*, *125*, e2020JA028198. https://doi.org/10.1029/2020JA028198

Received 6 MAY 2020
Accepted 21 JUL 2020
Accepted article online 11 AUG 2020

Abstract The Solar, Anomalous, and Magnetospheric Particle Explorer (SAMPEX) mission provided long-term measurements of 10s of megaelectron volt (MeV) inner belt ($L < 2$) protons (1992–2009) as did the Polar-orbiting Operational Environmental Satellite-18 (POES-18, 2005 to present). These long-term measurements at low-Earth orbit (LEO) showed clear solar cycle variations which anticorrelate with sunspot number. However, the magnitude of the variation is much greater than the solar cycle variation of galactic cosmic rays (>GeV) that are regarded as a source of these trapped protons. Furthermore, the proton fluxes and their variations sensitively depend on the altitude above the South Atlantic Anomaly (SAA) region. With respect to protons (>36 MeV) mirroring near the magnetic equator, both POES measurements and simulations show no obvious solar cycle variations at $L > 1.2$. This is also confirmed by recent measurements from the Van Allen Probes (2012–2019), but there are clear solar cycle variations and a strong spatial gradient of the proton flux below $L = 1.2$. A direct comparison between measurements and simulations leads to the conclusion that energy loss of trapped protons due to collisions with free and bound electrons in the ionosphere and atmosphere is the dominant mechanism for the strong spatial gradient and solar cycle variation of the inner belt protons. This fact is also key of importance for spacecraft and instrument design and operation in near-Earth space.

1. Introduction

Interplanetary space is permeated by galactic cosmic rays (GCRs), mostly protons with kinetic energies above hundreds of megaelectron volts (MeV). Most of these particles are likely produced by supernovae in our galaxy (e.g., Blasi, 2013). Soon after the discovery of Earth's Van Allen radiation belts six decades ago, it was recognized that the main source of inner belt ($L < 2$) protons, with kinetic energies of 10s of MeV to gigaelectron volt (GeV), is Cosmic Ray Albedo Neutron Decay (CRAND) (e.g., Dragt et al., 1966; Singer, 1958). In this process, cosmic rays (>GeV energies) interact with neutral atoms in the upper atmosphere to produce energetic albedo neutrons which decay into protons, electrons, and antineutrinos. Most of the kinetic energy is retained by the protons, and some of these consequently become geomagnetically trapped in the inner belt region.

Ground neutron monitor (NM) measurements, used to infer cosmic ray intensity variations even before the space age (e.g., Simpson, 2000), exhibit a strong geomagnetic latitude dependence. NMs at different geomagnetic latitudes have different cutoff energies for incoming cosmic rays, from 100s of MeV in the polar region to multi-GeV in the inner belt ($L < 2$, corresponding to geomagnetic latitude of <45°) (e.g., Selesnick et al., 2007; Smart & Shea, 2005). All NM data show a variation in cosmic rays on the 11-year sunspot cycle and the 22-year solar magnetic cycle. Occasionally, the Sun emits energetic particles (mostly protons) of sufficient energy and intensity to be significantly above the cosmic ray level. They are detected by NMs at high latitudes as well. Such episodic events, ranging from a few times in a year to a few times in a sunspot cycle, are termed "ground-level enhancements" (GLEs) (e.g., Poluianov et al., 2017; Simpson, 1990).

Solar energetic protons are another source of 10s of MeV protons trapped in the inner belt but from a different process: inward radial diffusion of pretrapped energetic protons at larger L (e.g., Selesnick et al., 2007).

During solar energetic particle (SEP) events, some protons can become trapped in the Earth's magnetosphere (e.g., Hudson et al., 1995; Looper et al., 2005; Lorentzen et al., 2002) and diffuse inward to $L < 2$, adding to the pre-existing trapped protons in the inner belt (Selesnick et al., 2014, 2016, 2018). The initial trapping process is understood, in principal, to be due to electric and magnetic field fluctuations affecting Störmer orbits (Störmer, 1955). Solar protons are more likely to become trapped deep inside Earth's magnetosphere if followed by a large interplanetary shock impact (Blake et al., 1992; Hudson et al., 1995). Efforts have been made to understand the initial entrance of solar energetic protons to different geomagnetic latitudes (cutoff) (e.g., Engel et al., 2016; Kress et al., 2004, 2010; Leske et al., 2001; Qin et al., 2019). Nonetheless, it is still uncertain how many solar protons can become trapped in the magnetosphere for a given SEP event (Selesnick et al., 2010). It was also recognized that the SEP contribution to trapped protons inside $L < 1.3$ through radial diffusion is insignificant (e.g., Jentsch, 1981; Selesnick & Albert, 2019).

Over the last four decades, Voyager 1 (V1) and Voyager 2 (V2), launched in 1977–1978 (https://voyager.jpl.nasa.gov/mission/status/), have been measuring cosmic rays in the heliosphere and beyond (e.g., Cummings et al., 2016). Figure 1 shows the long-term flux of energetic particles from the Cosmic Ray Subsystem (CRS) instrument (Stone et al., 1977) onboard V1 and V2 as they traveled from the inner heliosphere to the outer heliosphere and into the local interstellar medium. The top two panels show the differential flux of ~270–350 MeV/nuclei (mostly protons) measured by V1 and V2. The solar cycle variation of the cosmic rays is clear, almost in phase with the Thule NM measurement (second from last panel), particularly when V1 and V2 are not too far from the Earth, and in anticorrelation with the sunspot number (last panel). The solar cycle modulation of cosmic ray intensity was stronger in the inner heliosphere and got weaker as V1 and V2 traveled to the outer heliosphere. After they exited the heliosphere into the local interstellar medium, the solar cycle modulation virtually disappeared (more apparent on V1). Incoming cosmic rays are modulated by the solar wind, especially by stronger solar magnetic structures during solar maximum (e.g., Cane et al., 1999). The solar cycle modulation depends on the particles' energy and is greater for the lower energy particles (e.g., Usoskin et al., 2005).

In the rest of this paper, we focus on the characteristics of trapped inner belt protons (10s of MeV) based on long-term measurements from Solar, Anomalous, and Magnetospheric Particle Explorer (SAMPEX), Polar-orbiting Operational Environmental Satellite (POES), Van Allen Probes, and model simulations. We will show that the solar cycle variation of inner belt protons measured by low-Earth orbit (LEO) satellites is mainly due to losses from atmospheric collisions and that the inner belt proton intensity and solar cycle variation measured at LEO depend sensitively on altitude and thus the particle's pitch angle. Detailed comparison between POES measurements and model simulations for the protons mirroring near the magnetic equator shows a strong gradient in the proton flux. Its solar cycle variation is only obvious at $L < 1.2$, which is also confirmed by recent measurements from the Van Allen Probes (2012–2019) in geo-transfer-like orbit. It is remarkable that the general model simulations, in which the decay of the proton fluxes is mainly due to energy loss to free and bound electrons in the local plasma and neutral atmosphere and is solar cycle dependent (Selesnick & Albert, 2019), reproduce the measurement well. This leads to a consolidated understanding that the solar cycle variation of the ionospheric and atmospheric density dominates the observed solar cycle variation of trapped inner belt proton flux.

2. Observations and Discussions

2.1. SAMPEX Measurements

The SAMPEX mission was launched into a ~510 km × 690 km altitude and 82° inclination orbit in July of 1992. The altitude of SAMPEX decayed slowly for the first 8 years and faster afterwards, reaching 410 × 500 km by 2008; it re-entered the atmosphere on 13 November 2012 (Baker, Mazur, & Mason, 2012). In order to show the long-term variation of energetic protons at a given altitude, we plot the differential flux of 27.4- to 37.4-MeV protons measured by SAMPEX/PET (Cook et al., 1993) from late 1992 to late 2009 (when PET ceased operation) at an altitude around 500 km (±20 km) and $L = 1.33$–1.42 in the top panel of Figure 2. Also plotted in Figure 2 are the "Delaware" NM (L = ~2.4) measurements and the sunspot number. The solar cycle variation is obvious in the proton flux and the NM measurements created by GCR that reach the atmosphere at this magnetic latitude (50°, $L = 2.4$). However, the magnitude

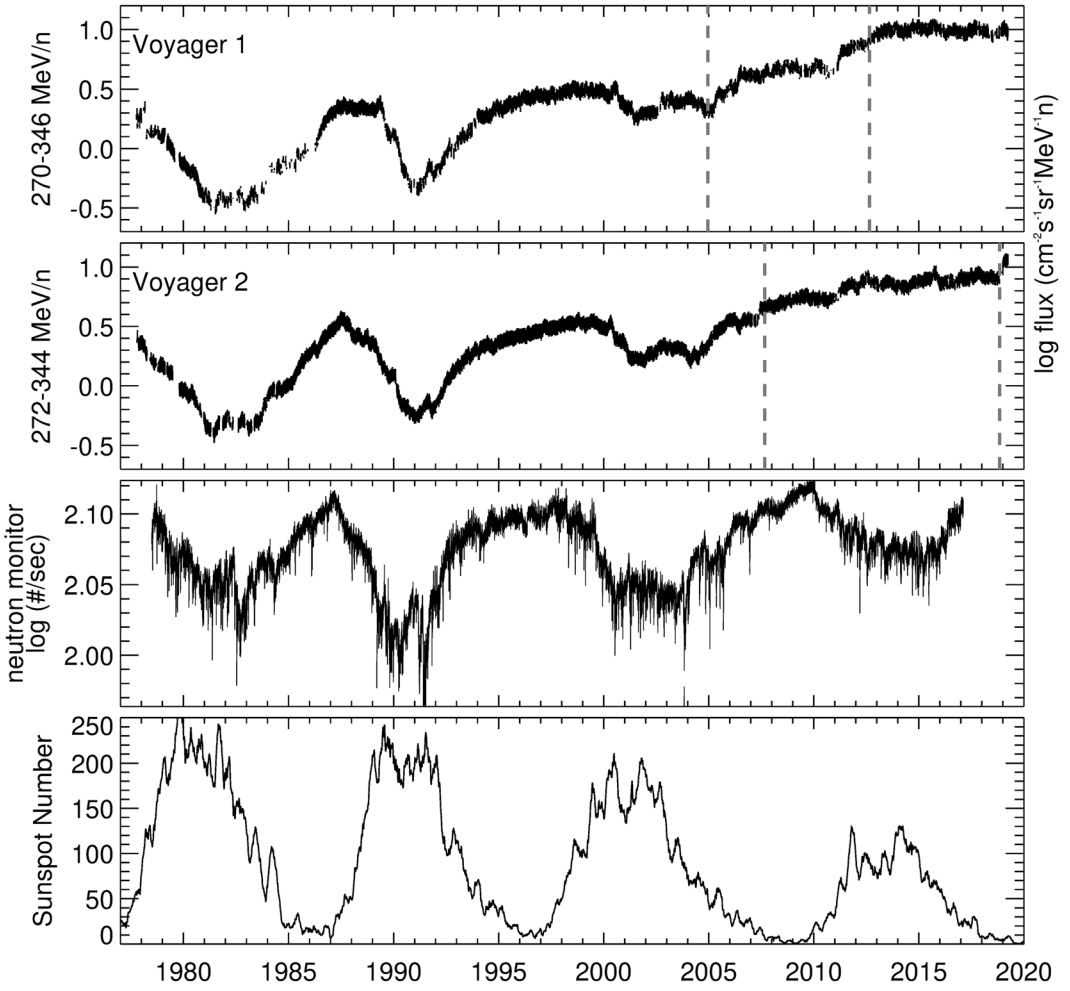

Figure 1. Long-term measurements of cosmic rays (mostly protons) by CRS onboard V1 and V2 (https://cdaweb.gsfc.nasa.gov) dashed vertical lines in the Voyager panels indicate the dates when the termination shock (TSX) and heliopause (HPX) was crossed (V1 TSX: 16 December 2004 at 94 AU, V1 HPX: 25 August 2012 at 121.6 AU; V2 TSX: 30 August 2007 at 83.65 AU, V2 HPX: 5 November 2018 at 119 AU). (1) V1/CRS measurements of 270–346 MeV/n of proton fluxes. Data points with values greater than 115% or less than 85% of the previous 50-day average fluxes are filtered out. (2) Similar to (1) but for V2/CRS measurements. (3) Daily averaged neutron count rate as measured by the neutron monitor located in Thule, Greenland (in the open field line region) (http://neutronm.bartol.udel.edu/). Data points with values greater than 105% or less than 95% of the previous 50-day average count rates are filtered. (4) 100-day running averaged sunspot number (ftp://spdf.gsfc.nasa.gov/pub/data/omni/).

of the variation is vastly different. For a GCR proton to reach the atmosphere in $L < 1.42$ (corresponding to a magnetic latitude of 33°) and $L = 2.4$, it would need to have an energy of >6 and ≥2.3 GeV, respectively (Selesnick et al., 2007; Smart & Shea, 2005). The modulation by the solar wind of multi-GeV GCR is limited, as shown by the relative variation of about 20% ([flux_max − flux_min]/flux_min) of the NM measurement (Panel 2) over a solar cycle (the relative variation of the NM at Mexico City, $L \sim 1.3$, is about 14.8%). However, the relative solar cycle variation of the satellite-measured proton flux (Panel 1) is about 300%, which suggests that the solar cycle variation of trapped inner belt protons is not due to this source. It was recognized earlier that the solar cycle variation of the upper atmosphere and ionosphere significantly influences low-altitude energetic protons (e.g., Huston & Pfitzer, 1998; Miyoshi et al., 2000; Qin et al., 2014). It is good to consolidate this understanding by comparing the trapped proton measurements with ground NM measurements at different latitudes and direct GCR measurements in the interplanetary space, although the 100s of MeV protons shown in Figure 1 can barely reach the atmosphere at the high latitudes (>60°) and even a higher rigidity (or energy) is required to reach the atmosphere at lower latitudes (e.g., Selesnick et al., 2007; Smart & Shea, 2005).

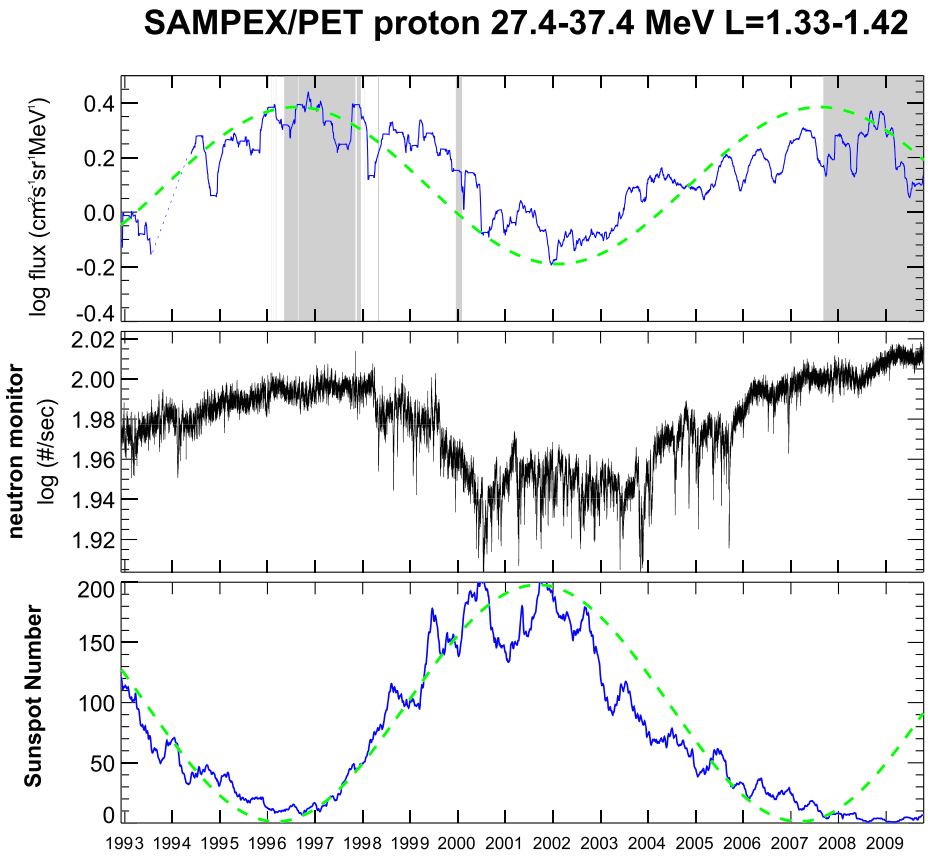

Figure 2. Top panel, long-term measurements of 27.4- to 37.4-MeV proton fluxes at L = 1.33–1.42 by SAMPEX/PET (http://www.srl.caltech.edu/sampex/DataCenter/) with a 100-day running average. Data points are only kept if they are close to 500 km in altitude (within a 20-km margin). Time periods marked by the gray background are when SAMPEX was spinning and data in these periods are multiplied by a factor of 2 in order to match the fluxes to those in the normal mode when SAMPEX was zenith pointing. Data from 21 September 1993 to 17 March 1994 are not reliable due to the satellite operation and are removed. (2) Daily averaged neutron count rates as measured by the neutron monitor located in Delaware, USA (L = ~2.4) (http://neutronm.bartol.udel.edu/). Data points with values greater than 105% or less than 95% of the previous 50-day averaged count rate are removed. (3) 100-day running average sunspot numbers. The dashed green curves on top and bottom panels are fitted sine curves with an 11-year period.

If we approximate the solar cycle variations of the measured proton flux (top panel of Figure 2) and sunspot number (bottom panel of Figure 2) by sine curves (dashed green lines) with an 11-year period, we can estimate that there exists a phase lag of 154 days between the sunspot number and the proton flux. This phase lag can be understood as how fast the trapped proton flux, which enhanced during solar min, decayed when the ionospheric and atmospheric densities increased during solar max. Obviously, the estimate of this phase lag has its uncertainty, and also this phase lag should be dependent on the altitude of measurements of the protons flux. Both aspects will be discussed next subsection.

2.2. POES Measurements

In comparison, we analyzed the long-term measurements from POES-18, which was launched on 20 May 2005, into a Sun-synchronous orbit (99.2° inclination) with an 848 km × 869 km altitude (Sandanger et al., 2015). There are only integral fluxes available before 2015 (Evans & Greer, 2004; https://satdat.ngdc.noaa.gov/sem/poes/data/). To plot the long-term measurements, we merged the integral flux (before 2015) and the differential flux (after 2015), displayed in top two panels in Figure 3. Sunspot number and $F10.7$ measurements (both daily averaged) are plotted in the bottom two panels. The solar cycle variation of the energetic proton flux is still obvious, but the relative variation of the proton flux, (flux_max − flux_min)/flux_min, at these higher altitudes is much smaller than the SAMPEX/PET measurements at lower

altitudes. The relative solar cycle variation is only about 21% for both >36- and >140-MeV protons, which suggests that loss from atmospheric collision is much smaller at this higher altitude.

If we approximate the solar cycle variations of the measured proton flux (Figure 3a) and sunspot numbers (Figure 3c) by sine curves with an 11-year period, we can estimate that there exists a phase lag of 730 days, which is much longer than the phase lag between the SAMPEX proton flux and the sunspot numbers. This much greater phase lag is consistent with the much smaller solar cycle variations exhibited by the POES measurements, which were taken at higher altitude (~860 km), where the influence of ionosphere and atmosphere is much weaker than at ~500 km and thus the residence time of the protons measured at ~860 km is much longer.

We also did the phase lag calculation for the >140-MeV protons (Figure 3b) in the same manner and found the same results as for >36-MeV protons. We would expect that there should be a longer phase lag for higher energy protons since they are less likely to be affected by the atmospheric density. However, we should also realize that the sine fitting is an approximate method, which has an uncertainty of 1 year (one grid of the points used for the fitting). Another point should be mentioned here is that the relative variations of the proton flux for these two panels over a solar cycle are about the same as well (~21%).

It is worth pointing out that the small periodic variation (~120-day periodicity) in the Figures 3a and 3b is associated with the precession of the orbit, with the peaks corresponding to apogee (869 km) in the Southern Hemisphere and above South Atlantic Anomaly (SAA) and the dips corresponding to perigee (848 km) in the Southern Hemisphere. The relative variation is 2.9% for >36-MeV protons and 2.7% for >140-MeV protons, even though the altitude difference is only 21 km. This detailed feature suggests that trapped inner belt protons have a strong altitude gradient, confirming early results (e.g., Parsignault et al., 1981). This spatial gradient also suggests that there would be an east-west asymmetry if measured by a unidirectional detector as the eastward traveling fluxes, whose guiding centers are at higher altitudes, are expected to be greater than the westward traveling fluxes, whose guiding centers are at lower altitudes because of the finite protons gyroradii (Heckman & Nakano, 1963; Lenchek & Singer, 1962). For example, the averaged flux for >36-MeV protons has a relative increase of 2.9% from 848 to 869 km above SAA ($J_{848} = J_{869} \exp[-21/h]$; $[J_{869} - J_{848}]/J_{848} = 0.029$). This gives the average scaleheight (h) of the proton flux around this region as ~735 km, which is far greater the gyroradius of a 36-MeV proton at this location

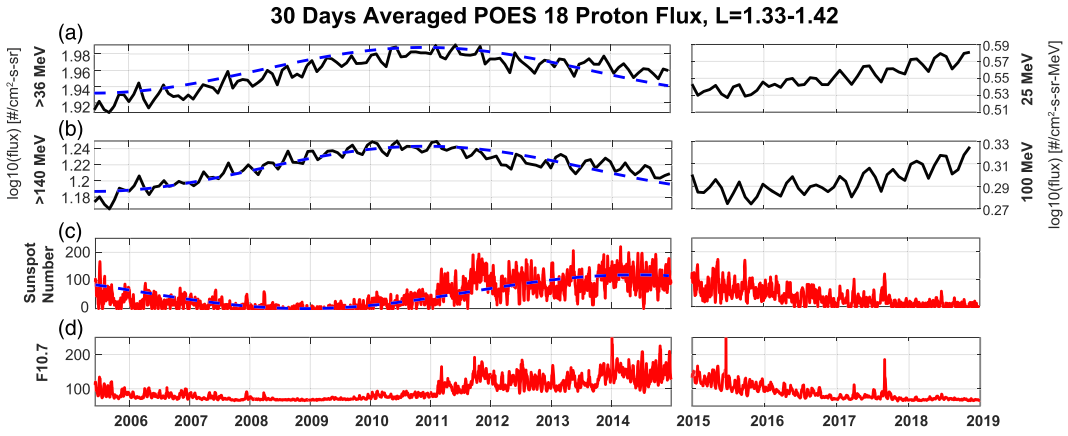

Figure 3. 30-day averaged proton flux at $L = 1.33–1.42$ during June 2015 to December 2018 measured by NOAA POES-18 satellite are plotted in Panel (a) (>36-MeV proton flux) and Panel (b) (>140-MeV proton flux); Panel (c) is the sunspot number; Panel (d) is the *F*10.7 solar index. Note that after 2014, there is no integral energy channel of proton flux in data product (https://satdat.ngdc.noaa.gov/sem/poes/data/; Evans & Greer, 2000). Thus, two nearby differential energy channels (25 and 100 MeV) of proton fluxes are presented on the right of this figure. The sunspot number and *F*10.7 solar indices are from OMNIWeb (ftp://spdf.gsfc.nasa.gov/pub/data/omni/). The *L* is directly obtained from the POES data product, which uses a current IGRF model for the epoch midway through the year the data were acquired. The magnetic calculations are updated once a year using the new IGRF model and satellite orbit information. The dashed blue curves on Panels a–c are fitted sine curves with an 11-year period.

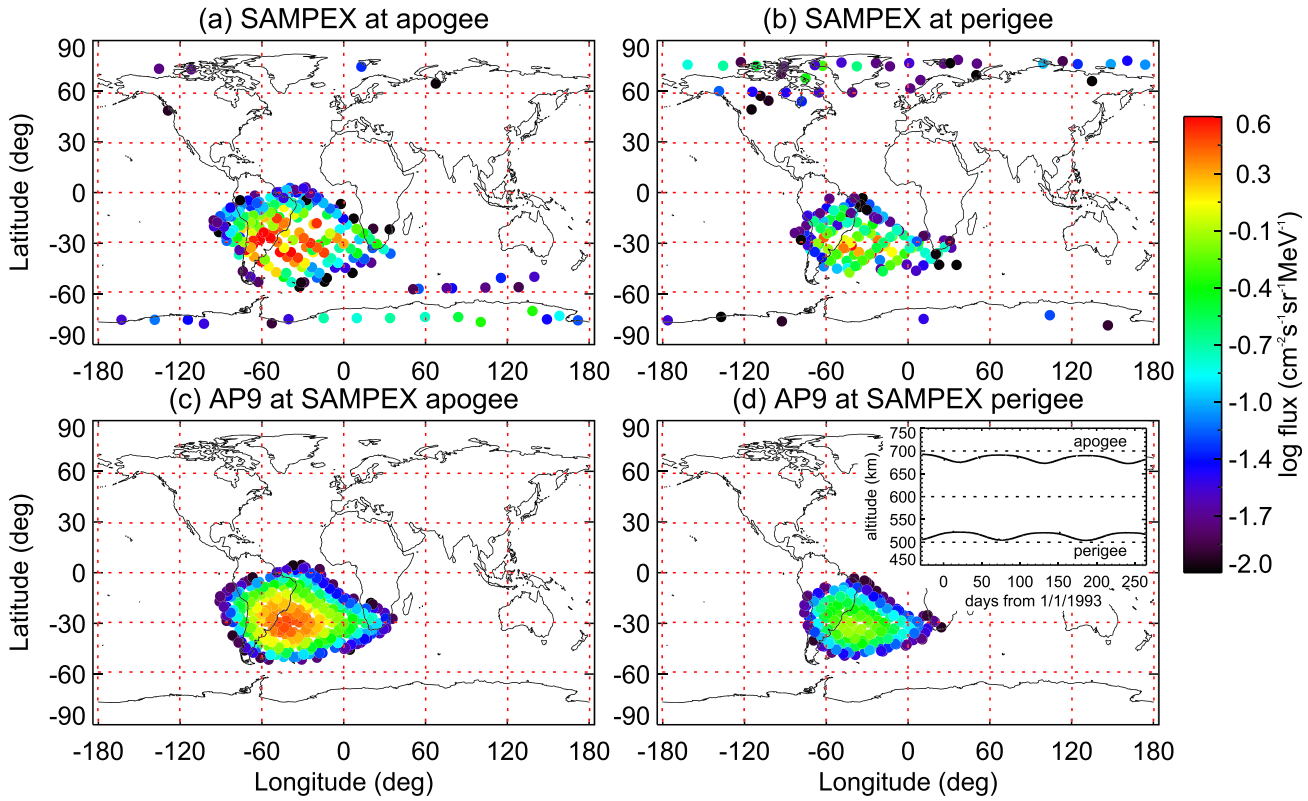

Figure 4. The insertion in Panel (d) shows the altitudes of SAMPEX's apogee and perigee for this time period. Panels (a) and (b) show the locations of SAMPEX/PET measurements of 27.4- to 37.4-MeV protons with flux greater than 0.01/(cm^2-s-sr-MeV) around its apogee (673.4–692.5 km) and perigee (504.9–522.1 km), respectively, between 3 December 1992 and 21 September 1993. The flux ratio between measurements taken around apogee and perigee is 1.85. Panels (c) and (d) show the 30-MeV proton flux (with a threshold of >0.01) from the AP9 model calculated at SAMPEX's location around apogee and perigee. The local pitch angles of these measurements were taken between 30° and 80°, corresponding to the local pitch angle coverage of the SAMPEX/PET measurements.

(~50 km). The eastward traveling flux would be ~15% higher than the westward traveling flux if measured by a unidirectional detector at this location.

However, the proton detectors on POES have a large field of view (FOV), 120° and 180° for >36 and >140 MeV, and the detectors are pointing toward the zenith directions. So the east-west asymmetry will not be significant from these detectors' measurements. In addition, we have averaged the measurements during their descending and ascending phases from many orbits for many days, so the east-west asymmetry will not affect the results presented here. It should be noted that the essence of east-west asymmetry are commonly considered in analysis of SEP events at or inside geostationary orbit (e.g., Filwett et al., 2020; Rodriguez et al., 2010), where the difference between eastward and westward fluxes can be over one-order magnitude because of the spatial gradient and the much larger gyroradius of SEP (at a weaker magnetic field).

We should also note that the results on Figure 3 are dominated by trapped populations, measured above SAA region (further illustrated in Figure 4), even though POES also measure drift/bounce loss cone particles, whose contributions are negligible.

2.3. Altitude Dependence and Comparison With AP9 Model

For highly inclined LEO spacecraft, the radiation dose is mainly due to inner belt protons, which increases with altitude because of the pitch angle distribution of the trapped protons. This altitude dependence is well recognized (e.g., Parsignault et al., 1981) and relates to mission design because of radiation effects on spacecraft (e.g., Miyake et al., 2014). The latest community-supported Aerospace Proton Model (AP9) has included this altitude dependence based on data from various missions, such as CRRES and Polar (Ginet et al., 2013. Also see https://www.vdl.afrl.af.mil/programs/ae9ap9/files/package/Ae9Ap9_v1_50_001_

ReleaseNotes.pdf). Here, we demonstrate the altitude dependence from SAMPEX/PET data of its first year's measurements and compare them with AP9 model results.

A highly inclined LEO spacecraft can only measure trapped inner belt particles when it traverses the SAA region and measures SEP only at high latitudes. SAMPEX's orbit had a procession period of ~110 days, with its apogee moving from the Southern Hemisphere to the Northern Hemisphere and back again.

The insert in Figure 4d shows the altitude of SAMPEX's apogee and perigee early in the mission. Figures 4a and 4b show the location of SAMPEX/PET measurements of 27.4- to 37.4-MeV protons with flux greater than 0.01/(cm^2-s-sr-MeV) around its apogee (673.4–692.5 km) and perigee (504.9–522.1 km), respectively, between 3 December 1992 and 21 September 1993. It is evident that most measurements of trapped protons were taken near the SAA, with much higher flux and more data points when apogee was in the Southern Hemisphere. It should be noted that measurements at high latitudes were during SEP events. The flux ratio between measurements taken around apogee and perigee is 1.85. This is almost a factor of two differences in radiation dose due to the proton flux between the altitude of 690 vs. 510 km for the same inclination. Figure 4 illustrates clearly that the radiation dose for a LEO spacecraft comes mostly from trapped inner belt protons around the SAA region, which is also important information for operating LEO spacecraft and instruments as they are all subject to such penetrating protons (e.g., Li et al., 2015), which have deleterious effects on various subsystems onboard and can affect intended measurements (e.g., Baker, 2002; Miyake et al., 2014).

Figures 4c and 4d show the 30-MeV proton flux (with a threshold of >0.01/[cm^2-s-sr-MeV]) from the AP9 model calculated at SAMPEX's location around its apogee and perigee. The local pitch angles of these measurements were taken to be between 30° and 80°, corresponding to the local pitch angle coverage of the SAMPEX/PET measurements. The flux ratio between apogee and perigee is 2.82, comparable to the actual SAMEPX/PET measurements.

It should be pointed out that the proton flux difference between the different altitudes is well reproduced by AP9 model. However, the solar cycle variation, which is much greater, with a flux ratio (maximum flux around solar min)/(minimum flux around solar max) of 4.5 around 500 km (as shown in Figure 2, top panel), is yet to be included in AP9 model (W. R. Johnston, private comm., 2019). The AP8 model has only two values for inner belt protons, corresponding to solar min and solar max. The same flux ratio of 30-MeV protons at $L = 1.4$ at 500 km is 1.6 (based on IRBEM-LIB, https://sourceforge.net/projects/irbem/), much smaller than what SAMPEX's measurements show in Figure 4.

2.4. Van Allen Probes/REPT Measurements

Van Allen Probes, a pair of identical spacecraft, were launched into a geo-transfer-like orbit, with perigees of ~600-km altitude and apogees around 5.8 R_E from the center of Earth and inclination of 10° on 30 August 2012 (Kessel et al., 2012; Mauk et al., 2012). The pulse-height-analyzed (PHA) data downloaded since October 2013 from the Relativistic Electron-Proton Telescope (REPT) (Baker, Kanekal et al., 2012; Spence et al., 2013) onboard the Van Allen Probes have been used to investigate the variation of 10s of MeV protons in the magnetosphere (Selesnick et al., 2014, 2016). The PHA data have also made it possible to extend the energy range of the original required measurements of REPT (24–76 MeV) to a much wider energy range: 18–600 MeV (Selesnick et al., 2018).

REPT, mounted on the side of the spacecraft that spins along the Sun-pointing axis, has a FOV of 32° and can measure particles with all equatorial pitch angles in the inner belt after a spin period (~11 s) (Baker, Kanekal et al., 2012). Figure 5a shows the 10-day averaged 27-MeV proton flux with equatorial pitch angles between 75–90° (black line) and 35–55° (blue line) at $L = 1.3$–1.4. The measured protons represented by the black line are stably trapped since the largest drift loss cone, in terms of equatorial pitch angle, at $L = 1.3$ is about 50° (which means a charged particle with an equatorial pitch angle just less than this would reach <100-km altitude in SAA and be lost into atmosphere). The protons represented by the blue line include both stably trapped protons (but closer to the drift loss cone) and quasi-trapped protons (with equatorial pitch angles less than 50°), which would be lost within a drift period. The pointing direction of the center of the FOV of REPT versus the local magnetic field can be accurately determined, but the angular resolution is still 16° from the pointing direction. The proton flux represented by the blue line, which is about one order of magnitude lower than the proton flux represented by the black line, not only includes protons with small equatorial pitch angles but also includes background from higher energy protons (Selesnick et al., 2018).

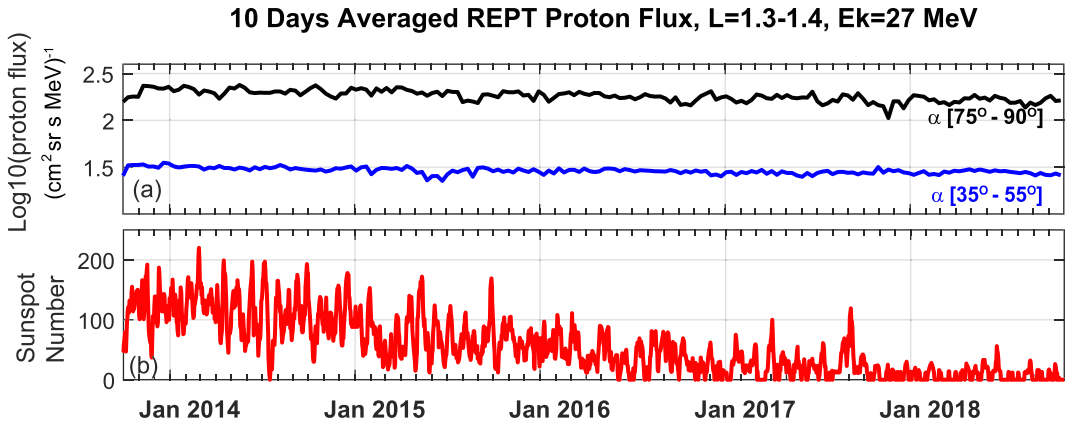

Figure 5. Proton fluxes determined from REPT/PHA data (Selesnick et al., 2014, 2018) measured by Van Allen Probes/REPT are plotted in Panel (a): 10-day averaged 27-MeV proton flux at $L = 1.3$–1.4 during October 2013 to October 2018. The L bin is 0.1, the energy resolution is 4 MeV, and the equatorial pitch angle resolution is 7.2°. The black curve and blue curve present the average proton flux in equatorial pitch angle range 75–90° and (35–55°, respectively; Panels (b): daily averaged sunspot number.

The background contribution to the blue line becomes significant but still negligible for the black line, as demonstrated in Figs. 3 and 4 in Selesnick et al. (2014).

It should be pointed out that the proton flux, in Figure 5a, with larger equatorial pitch angles (black line) is much greater than the proton flux with smaller equatorial pitch angles. Neither the black nor blue line shows any discernible solar cycle variation similar to that seen in the SAMPEX and POES data (Figures 2 and 3). This suggests that the sources and losses of inner belt protons mirroring close to the magnetic equator are different from those of inner belt protons measured at LEO. The latter have smaller equatorial pitch angles and a lower flux; they reach lower altitudes, thus subjecting them more to energy loss and pitch angle scattering from atmospheric collisions. In fact, trapped protons mirroring near the magnetic equator do show a solar cycle variation at lower L and a strong spatial gradient in their flux and variation at $L < 1.2$, as is discussed next.

2.5. Comparison Between Measurements and Model Results at Low L for Equatorially Mirroring Protons

Figure 6 shows the omnidirectional >36-MeV proton flux from June 2005 to February 2018 from POES-18 observations taken only near the magnetic equator with $B/B_{min} < 1.01$ (where B_{min} is the magnetic field strength at the equator, based on the POES-18 orbit and the IGRF model), the corresponding simulation results based on a theoretical model (Selesnick & Albert, 2019), and REPT PHA data which are also converted to >36-MeV fluxes near the magnetic equator for direct comparison.

The simulation is based on the model described in Selesnick et al. (2007) with an extra loss equivalent to a mean lifetime of 22 years for the trapped protons (Selesnick & Albert, 2019), in addition to including energy loss due to collisions with free and bound electrons in the ambient plasma and neutral atmosphere, the direct loss due to inelastic nuclear scattering and detrapping during magnetic storms. The sources in the model are from CRAND and trapped energetic solar protons. The CRAND source rate is $S_n = <j_n>/(v\ r\ T_n)$, where v is neutron speed, T_n is the mean lifetime of a neutron, 887 s, and r is the relativistic factor for a given neutron energy. The neutron intensity j_n is drift averaged ($<j_n>$), and itself is evaluated at the geographic location where the negative tangent to the trapped proton trajectory intersects the top of the atmosphere (100-km altitude). The energetic source neutron must be coming from the Earth (thus CRAND) and have the same direction of the proton, which attains the full kinetic energy and moves in the same direction as the decaying neutron. If there is no intersection for a given point on the trajectory then $j_n = 0$. The CRAND source for the inner radiation belt comes mostly from low geomagnetic latitude or high cutoff rigidity. The low-latitude neutron flux is relatively insensitive to solar cycle modulation because of the high cutoff rigidity (the GCR source corresponding to multiple GeV protons, which vary little over a solar

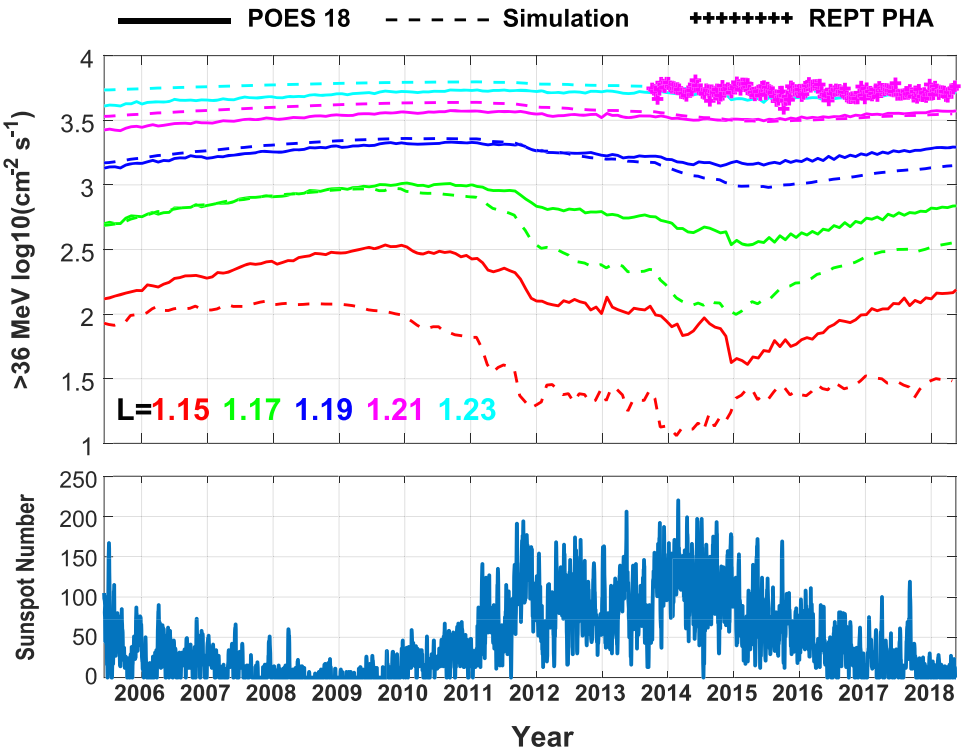

Figure 6. Top panel: omnidirectional integral fluxes of >36-MeV protons mirroring near the magnetic equator with $B/B_{min} < 1.01$ for different L (color-coded). Solid lines, from June 2005 to February 2018, are from POES-18 P7–P9 sensor, which are omnidirectional solid-state detectors with 120° FOV for P7 and 180° FOV for P8 and P9 (Evans & Greer, 2004). The geometric factors used to convert the count rate of omnidirectional solid-state detectors to the flux are obtained from appendix F of Evans and Greer (2004). After 2015, only differential fluxes from POES-18 are available, the integral fluxes here are calculated from raw format POES-18 data (https://satdat.ngdc.noaa.gov/sem/poes/data/raw/ngdc/), and a factor of 0.85 is multiplied to the calculated integral fluxes to ensure a smooth transition between the end of 2014 and the start of 2015; dashed lines are for simulation results based on a theoretical model (Selesnick et al., 2007; Selesnick & Albert, 2019); the "+" dots are for Van Allen Probes/REPT PHA data (for $L = 1.21$ only) from October 2013 to February 2018. Bottom panel: daily averaged sunspot numbers. Due to offset of the Earth's center and dipole center, POES-18 is able to cross the magnetic equator at different L (up to $L = 1.23$) at different longitudes.

cycle). As for the SEP source, statistical studies of the injection efficiency as a function L, energy, and equatorial pitch angle are not yet available. Trajectory tracing simulations show how solar ion trapping and transport to low L occurs (Hudson et al., 1997, 2004; Kress et al., 2005). The solar proton source rate is approximated as step function in L, $S_p > 0$ at $L \geq 2$ and $S_p = 0$ at $L < 2$. More detailed description is available in Selesnick et al. (2007). Radial diffusion is not included in the model here (for Figure 6) due to the very weak and uncertain radial diffusion rate at $L < 1.25$ (e.g., Schulz & Lanzerotti, 1974). The initial condition of this simulation was set 10 years ago. However, because we focus on 10s of MeV protons at lower L regions, the loss process is rather dynamic (while the source is stable), the simulation results quickly lose memory of their initial values, reaching a dynamic balance of the current source and loss.

The REPT PHA data were first processed to obtain the differential unidirectional proton flux as a function of the kinetic energy and the L value of the proton guiding center and the equatorial pitch angle and were averaged over consecutive daily intervals (Selesnick et al., 2018; Selesnick & Albert, 2019). The differential unidirectional proton fluxes were integrated over equatorial pitch angles (following the eq. 5 of Selesnick et al. (2014)) to obtain omnidirectional proton fluxes and were integrated over kinetic energy to obtain the integral proton flux shown in Figure 6.

We note several outstanding features in Figure 6:

1. The REPT PHA flux compares well with POES flux when both of them are restricted to near the magnetic equator, which is remarkable considering the different instrument designs operating in different orbits.

2. The simulation results reproduce well the POES measurements for the main features: (i) no obvious solar cycle variation at $L > 1.2$ but clear solar cycle variation at $L < 1.2$ and the magnitude of the variation greatly enhance at lower L, e.g., over one order of magnitude variation at $L = 1.15$ between solar max and min; (ii) a strong spatial gradient of the proton flux at $L < 1.2$, e.g., over one order of magnitude difference in flux between protons drifting at $L = 1.15$ and $L = 1.17$ near the magnetic equator (the spatial difference between these two drift shells is ~120 km); (iii) the spatial gradient itself is a strong function of L, increasing significantly at lower L and decreasing at $L > 1.2$.
3. The phase lags between the proton flux (both simulation results and POES measurements) and the sunspot number are strikingly different at different L. There is little phase lag at $L = 1.15$ (particularly in the simulation results), suggesting that proton energy loss is fast at low altitude (above the magnetic equator) and greatly enhanced during solar max (when the local atmospheric density enhanced). However, as L increases slightly, e.g., to $L = 1.17$ and $L = 1.19$ (equivalent to ~120-km distance between these two drift shells), the phase lag increases significantly. The phase lag between the simulation results and the sunspot number is estimated in a similar way in Figures 2 and 3, 37 days (229 days for POES), 165 days (357 days for POES), and 485 days (485 days for POES) for $L = 1.15$, 1.17, and 1.19, respectively.

For protons mirroring close to the magnetic equator, there is no obvious solar cycle variation at $L > 1.2$. This is very different from measurements taken at higher latitudes (as demonstrated in Figures 2 and 3, $L = 1.33$–1.42) where the solar cycle variation is mainly due to enhanced loss of protons, which have smaller equatorial pitch angles and are already close to the drift loss cone, during solar max.

In the simulation model, there are several loss terms for the protons: energy loss due to collisions with free and bound electrons in the ambient plasma and neutral atmosphere, direct loss due to inelastic nuclear scattering, and detrapping during magnetic storms. In the low L region (<1.25), detrapping is negligible, and the inelastic nuclear scattering is not significantly compared to the energy loss due to collisions with free and bound electrons, which is the dominate loss mechanism and increases fast at lower L. The source in this low L region is dominated by CRAND, as trapped energetic solar protons can hardly be radially diffused into such a low L region (Selesnick & Albert, 2019).

3. Summary and Conclusions

Motivated by the long-term measurements of GCR by V1 and V2, which show a clear solar cycle variation for ~300-MeV protons, we have investigated the solar cycle variations and local spatial variations of the trapped inner radiation belt protons. Based on the long-term measurements from SAMPEX, POES, and Van Allen Probes, we have demonstrated that the solar cycle variation of inner belt protons measured by LEO satellites is mainly due to enhanced loss during solar max since the variation of the corresponding cosmic rays (inferred from NM measurements at low latitude) is much smaller. We have also demonstrated that the inner belt proton intensity and solar cycle variation measured at LEO also depends sensitively on altitude. Such behavior of inner belt protons was predicted by theory decades ago (e.g., Blanchard & Hess, 1964) simply based on the source and loss mechanisms and also demonstrated with various satellites measurements (e.g., Huston & Pfitzer, 1998; Parsignault et al., 1981). Here, we have revisited this behavior and analyzed it in more quantitative detail, including comprehensive modeling of protons mirroring near the magnetic equator with direct comparison to measurements. Specific findings are as follows:

1. The flux ratio between measurements taken by SAMPEX around its apogee (690 km) and perigee (510) is 1.85, which is comparable to the AP9 model results (2.85) for the same altitudes. However, the flux ratio, (flux around solar min)/(flux around solar max), is 4.5 around 500 km from the solar cycle variation, which is not yet included in AP9 model. The same flux ratio of 30-MeV protons at $L = 1.4$ at 500 km from the solar cycle variation is only 1.6 based on AP8 model.
2. The relative solar cycle variation of the energetic proton flux at higher altitude (~860 km) becomes much smaller: only about 21.5% for >36-MeV protons and 21.4% for >140-MeV protons, suggesting that loss from the ionosphere and atmosphere becomes much less effective at higher altitudes.
3. The phase lags between the variation of the proton fluxes measured at LEO and the sunspot number increase significantly with the altitude of the measurement. The estimated phase lags are 154 days for SAMPEX measurements at ~500 km and 730 days for POES-18 measurements at ~860 km, again suggesting that loss from the ionosphere and atmosphere becomes much less effective at higher altitudes.

4. Another detailed feature of the sensitive dependence of the proton flux on altitude is demonstrated by POES-18 measurements. With a difference of only 21 km between POES-18's apogee (869 km) and perigee (848 km), the relative variation of >36-MeV protons and >140-MeV protons near apogee and perigee in the Southern Hemisphere is 2.9% and 2.7%, respectively.
5. For the protons mirroring near the magnetic equator, both measurements and simulations show no obvious solar cycle variation at $L > 1.2$ but there are clear solar cycle variations at $L < 1.2$ and a strong spatial gradient of the proton fluxes and its variations as well at $L < 1.2$. The phase lag between the proton flux and sunspot number increases greatly from $L = 1.15$ to $L = 1.19$.

Based on the good comparison between the simulation and the measurements of protons mirroring near the magnetic equator, we conclude that the decay of the measured proton flux is mainly due to the energy loss of protons colliding with free and bound electrons in the ionosphere and atmosphere and this energy loss is strongly altitude dependent, as demonstrated in Figure 6. As discussed in (Selesnick & Albert, 2019), the specific mechanism responsible for the extra loss term equivalent to a mean lifetime of 22 years in the model is still elusive, which presents a challenging and unanswered question as to the actual physical mechanisms responsible for the loss of these trapped protons. Nonetheless, the finding of fast energy loss of the protons at low altitude due to collisions with free and bound electrons in the ionosphere and atmosphere holds, and these demonstrated characteristics are also important for future spacecraft and instrument design and operation in this space environment.

Data Availability Statement

The data for Voyager, Neutron Monitor, SAMPEX, and POES are all publicly available at https://cdaweb.gsfc.nasa.gov, http://neutronm.bartol.udel.edu/, http://www.srl.caltech.edu/sampex/DataCenter/, and https://satdat.ngdc.noaa.gov/sem/poes/data/, respectively. Van Allen Probes REPT Level-1 data are available at www.rbsp-ect.lanl.gov. The sunspot number, $F10.7$ solar indices, and geomagnetic indices used in this study are obtained from the OMNI database (http://omniweb.gsfc.nasa.gov).

Acknowledgments
We are indebted to Richard Selesnick for providing the processed REPT PHA proton data and the simulation results for a direct comparison with POES measurements and multiple discussions. We would also like to thank Alan Cummings and Eric Christian for insightful discussions about GCRs and anomalous GCRs and Stuart Huston and Bob Johnson for insightful discussions regarding POES measurements and AP9 model. This work was supported in part by NSF grant AGS 1834971 and NASA grants: NNX17AD85G and NSSC19K0237 and by NASA/RBSPECT funding through JHU/APL contract 967399 under prime NASA contract NAS5-01072. ZX also acknowledges the support from the NSFC grant 41904143 and the China Postdoctoral Science Foundation Projects 2019M662700.

References

Baker, D. N. (2002). How to cope with space weather. *Science*, *297*, 1486.

Baker, D. N., Kanekal, S. G., Hoxie, V. C., Batiste, S., Bolton, M., Li, X., et al. (2012). The Relativistic Electron-Proton Telescope (REPT) instrument on board the Radiation Belt Storm Probes (RBSP) spacecraft: Characterization of Earth's radiation belt high-energy particle populations. *Space Science Reviews*, *179*(1–4), 337–381. https://doi.org/10.1007/s11214-012-9950-9

Baker, D. N., Mazur, J. E., & Mason, G. (2012). SAMPEX to reenter atmosphere: Twenty-year mission will end. *Space Weather*, *10*, S05006. https://doi.org/10.1029/2012SW000804

Blake, J. B., Kolasinski, W. A., Fillius, R. W., & Mullen, E. G. (1992). Injection of electrons and protons with energies of tens of MeV into $L < 3$ on March 24, 1991. *Geophysical Research Letters*, *19*(8), 821–824. https://doi.org/10.1029/92GL00624

Blanchard, R. C., & Hess, W. N. (1964). Solar cycle changes in inner zone protons. *Journal of Geophysical Research*, *69*, 3927.

Blasi, P. (2013). The origin of galactic cosmic rays (review article). *Astronomy and Astrophysics Review*, *21*(1), 70. https://doi.org/10.1007/s00159-013-0070-7

Cane, H. V., Wibberenz, G., Richardson, I. G., & von Rosenvinge, T. T. (1999). Cosmic ray modulation and the solar magnetic field. *Geophysical Research Letters*, *26*(5), 565–568.

Cook, W. R., Cummings, A. C., Cummings, J. R., Garrard, T. L., Kecman, B., Mewaldt, R. A., et al. (1993). PET: A proton/electron telescope for studies of magnetospheric, solar, and galactic particles. *IEEE Transactions on Geoscience and Remote Sensing*, *31*(3), 565–571. https://doi.org/10.1109/36.225523

Cummings, A. C., Stone, E. C., Heikkila, B. C., Lal, N., Webber, W. R., Johannesson, G., et al. (2016). Galactic cosmic rays in the local interstellar medium: Voyager 1 observations and model results. *The Astrophysical Journal*, *831*(1), 18 (21pp). https://doi.org/10.3847/0004-637X/831/1/18

Dragt, A. J., Austin, M. M., & White, R. S. (1966). Cosmic ray and solar proton albedo neutron decay injection. *Journal of Geophysical Research*, *71*(5), 1293–1304. https://doi.org/10.1029/JZ071i005p01293

Engel, M. A., Kress, B. T., Hudson, M. K., & Selesnick, R. S. (2016). Comparison of Van Allen Probes radiation belt proton data with test particle simulation for the 17 March 2015 storm. *Journal of Geophysical Research: Space Physics*, *121*, 11,035–11,041. https://doi.org/10.1002/2016JA023333

Evans, D. S., & Greer, M. S. (2000). Polar orbiting environmental satellite space environment monitor-2: Instrument descriptions and archive data documentation, NOAA Technical Memorandum, Boulder, Colorado OAR SEC 93, 93, version **1.4**, January 2000.

Evans, D. S., & Greer, M. S. (2004). Polar orbiting environmental satellite space environment monitor-2: Instrument descriptions and archive data documentation, NOAA Technical Memorandum, Boulder, Colorado OAR SEC 93, 93, version **1.4b**, January 2004.

Filwett, R. J., Jaynes, A. N., Baker, D. N., Kanekal, S. G., Kress, B., & Blake, J. B. (2020). Solar energetic proton access to the near-equatorial inner magnetosphere. *Journal of Geophysical Research: Space Physics*, *125*, e2019JA027584. https://doi.org/10.1029/2019JA027584

Ginet, G. P., O'Brien, T. P., Huston, S. L., Johnston, W. R., Guild, T. B., Friedel, R., et al. (2013). AE9, AP9 and SPM: New models for specifying the trapped energetic particle and space plasma environment. *Space Science Reviews*, *179*(1–4), 579–615. https://doi.org/10.1007/s11214-013-9964-y

Heckman, H. H., & Nakano, G. H. (1963). East-west asymmetry in the flux of mirroring geomagnetically trapped protons. *Journal of Geophysical Research*, *68*(8), 2117–2120. https://doi.org/10.1029/JZ068i008p02117

Hudson, M. K., Elkington, S. R., Lyon, J. G., Marchenko, V. A., Roth, I., Temerin, M., et al. (1997). Simulations of proton radiation belt formation during storm sudden commencements. *Journal of Geophysical Research*, *102*(A7), 14,087–14,102. https://doi.org/10.1029/97JA03995

Hudson, M. K., Kotelnikov, A. D., Li, X., Roth, I., Temerin, M., Wygant, J., et al. (1995). Simulation of proton radiation belt formation during the March 24, 1991 SSC. *Geophysical Research Letters*, *22*(3), 291–294. https://doi.org/10.1029/95GL00009

Hudson, M. K., Kress, B. T., Mazur, J. E., Perry, K. L., & Slocum, P. L. (2004). 3D modeling of shock-induced trapping of solar energetic particles in the Earth's magnetosphere. *Journal of Atmospheric and Solar - Terrestrial Physics*, *66*(15-16), 1389–1397. https://doi.org/10.1016/j.jastp.2004.03.024

Huston, S. L., & Pfitzer, K. A. (1998). A new model for the low altitude trapped proton environment. *IEEE Transactions on Nuclear Science*, *45*(6).

Jentsch, V. (1981). On the role of external and internal source in generating energy and pitch angle distributions of inner-zone protons. *Journal of Geophysical Research*, *86*(A2), 701–710. https://doi.org/10.1029/JA086iA02p00701

Kessel, R. L., Fox, N. J., & Weiss, M. (2012). The Radiation Belt Storm Probes (RBSP) and space weather. *Space Science Reviews*, *179*(1-4), 531–543. https://doi.org/10.1007/s11214-012-9953-6

Kress, B., Hudson, M., Perry, K., & Slocum, P. (2004). Dynamic modeling of geomagnetic cutoff for the 23–24 November 2001 solar energetic particle event. *Geophysical Research Letters*, *31*, L04808. https://doi.org/10.1029/2003GL018599

Kress, B., Mertens, C., & Wiltberger, M. (2010). Solar energetic particle cutoff variations during the 29–31 October 2003 geomagnetic storm. *Space Weather*, S05001. https://doi.org/10.1029/2009SW000488

Kress, B. T., Hudson, M. K., & Slocum, P. L. (2005). Impulsive solar energetic ion trapping in the magnetosphere during geomagnetic storms. *Geophysical Research Letters*, *32*, L06108. https://doi.org/10.1029/2005GL022373

Lenchek, A. M., & Singer, S. F. (1962). Effects of the finite gyroradii of geomagnetically trapped protons. *Journal of Geophysical Research*, *67*(10), 4073–4075. https://doi.org/10.1029/JZ067i010p04073

Leske, R., Mewaldt, R., Stone, E., & Rosenvinge, T. (2001). Observations of geomagnetic cutoff variations during solar energetic particle events and implications for the radiation environment at the space station. *Journal of Geophysical Research*, *106*(A12), 30,011–30,022. https://doi.org/10.1029/2000JA000212

Li, X., Selesnick, R. S., Baker, D. N., Jaynes, A. N., Kanekal, S. G., Schiller, Q., et al. (2015). Upper limit on the inner radiation belt MeV electron intensity. *Journal of Geophysical Research: Space Physics*, *120*, 1215–1228. https://doi.org/10.1002/2014JA020777

Looper, M. D., Blake, J. B., & Mewaldt, R. A. (2005). Response of the inner radiation belt to the violent Sun-Earth connection of October–November 2003. *Geophysical Research Letters*, *32*, L03S06. https://doi.org/10.1029/2004GL021502

Lorentzen, K. R., Mazur, J. E., Looper, M. D., Fennell, J. F., & Blake, J. B. (2002). Multisatellite observations of MeV ion injections during storms. *Journal of Geophysical Research*, *107*(A9), 1231. https://doi.org/10.1029/2001JA000276

Mauk, B. H., Fox, N. J., Kanekal, S. G., Kessel, R. L., Sibeck, D. G., & Ukhorskiy, A. (2012). Science objectives and rationale for the radiation belt storm probes mission. *Space Science Reviews*, *179*(1-4), 3–27. https://doi.org/10.1007/s11214-012-9908-y

Miyake, W., Miyoshi, Y., & Matsuoka, A. (2014). On the spatial of proton radiation belt from solar cell output variation of the Akebono satellite. *Advances in Space Research*, *53*(11), 1603–1609. https://doi.org/10.1016/j.asr.2014.03.002

Miyoshi, Y., Morioka, A., & Misawa, H. (2000). Long term modulation of low altitude proton radiation belt by the Earth's atmosphere. *Geophysical Research Letters*, *27*(14), 2169–2172. https://doi.org/10.1029/1999GL003721

Parsignault, D. R., Holeman, E., & Filz, R. C. (1981). Solar cycle induced modulation of the 55-MeV proton fluxes at low altitudes. *Journal of Geophysical Research*, *115*(A13), 11,439–11,442.

Poluianov, S. V., Usoskin, I. G., Mishev, A. L., Shea, M. A., & Smart, D. F. (2017). GLE and sub-GLE redefinition in the light of high-altitude polar neutron monitors. *Solar Physics*, *292*(11), 176. https://doi.org/10.1007/s11207-017-1202-4

Qin, M., Zhang, X., Ni, B., Song, H., Zou, H., & Sun, Y. (2014). Solar cycle variations of trapped proton flux in the inner radiation belt. *Journal of Geophysical Research: Space Physics*, *119*, 9658–9669. https://doi.org/10.1002/2014JA020300

Qin, M., Hudson, M., Kress, B., Selesnick, R., Engel, M., Li, Z., & Shen, X. (2019). Investigation of solar proton access into the inner magnetosphere on 11 September 2017. *Journal of Geophysical Research: Space Physics*, *124*, 3402–3409. https://doi.org/10.1029/2018JA026380

Rodriguez, J. V., Onsager, T. G., & Mazur, J. E. (2010). The east-west effect in solar proton flux measurements in geostationary orbit: A new GOES capability. *Geophysical Research Letters*, *37*, L07109. https://doi.org/10.1029/2010GL042531

Sandanger, M. I., Ødegaard, L.-K. G., Tyssøy, H. N., Stadsnes, J., Søraas, F., Oksavik, K., & Aarsnes, K. (2015). In-flight calibration of NOAA POES proton detectors—Derivation of the MEPED correction factors. *Journal of Geophysical Research: Space Physics*, *120*, 9578–9593. https://doi.org/10.1002/2015JA021388

Schulz, M., & Lanzerotti, L. J. (1974). *Particle diffusion in the radiation belts*. New York: Springer. https://doi.org/10.1007/978-3-642-65675-0

Selesnick, R. S., & Albert, J. M. (2019). Variability of the proton radiation belt. *Journal of Geophysical Research: Space Physics*, *124*, 5516–5527. https://doi.org/10.1029/2019JA026754

Selesnick, R. S., Baker, D. N., Jaynes, A. N., Li, X., Kanekal, S. G., Hudson, M. K., & Kress, B. T. (2014). Observations of the inner radiation belt: CRAND and trapped solar protons. *Journal of Geophysical Research: Space Physics*, *119*, 6541–6552. https://doi.org/10.1002/2014JA020188

Selesnick, R. S., Baker, D. N., Jaynes, A. N., Li, X., Kanekal, S. G., Hudson, M. K., & Kress, B. T. (2016). Inward diffusion and loss of radiation belt protons. *Journal of Geophysical Research: Space Physics*, *121*, 1969–1978. https://doi.org/10.1002/2015JA022154

Selesnick, R. S., Baker, D. N., Kanekal, S. G., Hoxie, V. C., & Li, X. (2018). Modeling the proton radiation belt with Van Allen Probes Relativistic Electron-Proton Telescope data. *Journal of Geophysical Research: Space Physics*, *123*, 685–697. https://doi.org/10.1002/2017JA024661

Selesnick, R. S., Hudson, M. K., & Kress, B. T. (2010). Injection and loss of inner radiation belt protons during solar proton events and magnetic storms. *Journal of Geophysical Research*, *115*, A08211. https://doi.org/10.1029/2010JA015247

Selesnick, R. S., Looper, M. D., & Mewaldt, R. A. (2007). A theoretical model of the inner proton radiation belt. *Space Weather*, *5*, S04003. https://doi.org/10.1029/2006SW000275

Simpson, J. A. (1990). Astrophysical phenomena discovered by cosmic ray and solar flare ground level events: The early years. *Proc. Int. Cosmic Ray Conf.*, *12*, 187.

Simpson, J. A. (2000). The cosmic ray nucleonic component: The invention and scientific uses of the neutron monitor. *Space Science Reviews*, *93*(1/2), 11–32. https://doi.org/10.1023/A:1026567706183

Singer, S. F. (1958). "Radiation belt" and trapped cosmic-ray albedo. *Physical Review Letters*, *1*(5), 171–173. https://doi.org/10.1103/PhysRevLett.1.171

Smart, D. F., & Shea, M. A. (2005). A review of geomagnetic cutoff rigidities for Earth-orbiting spacecraft. *Advances in Space Research*, *36*(10), 2012–2020. https://doi.org/10.1016/j.asr.2004.09.015

Spence, H. E., Reeves, G. D., Baker, D. N., Blake, J. B., Bolton, M., Bourdarie, S., et al. (2013). Science goals and overview of the Radiation Belt Storm Probes (RBSP) energetic particle, composition, and thermal plasma (ECT) suite on NASA's Van Allen Probes mission. *Space Science Reviews*, *179*(1-4), 311–336. https://doi.org/10.1007/s11214-013-0007-5

Stone, E. C., Vogt, R. E., McDonald, F. B., Teegarden, B. J., Trainor, J. H., Jokipii, J. R., & Webber, W. R. (1977). Cosmic ray investigation for the Voyager missions; energetic particle studies in the outer heliosphere—And beyond. *Space Science Reviews*, *21*, 355.

Störmer, C. (1955). *The polar aurora*. Oxford: Clarendon Press.

Usoskin, I. G., Alanko-Huotari, K., Kovaltsov, G. A., & Mursula, K. (2005). Heliospheric modulation of cosmic rays: Monthly reconstruction for 1951–2004. *Journal of Geophysical Research*, *110*, A12108. https://doi.org/10.1029/2005JA011250